Preparation of Novel Fluoroalkyl End-Capped Trimethoxyvinylsilane Oligomeric Nanoparticle-Encapsulated Binaphthol: Encapsulated Binaphthol Remaining Thermally Stable Even at 800 °C

Hideo Sawada,*[1] Yusuke Matsuki,[1] Yuki Goto,[1] Shun Kodama,[2] Masashi Sugiya,[2] and Yusuke Nishiyama[3]

[1]Department of Frontier Materials Chemistry, Graduate School of Science and Technology, Hirosaki University, Bunkyo-cho, Hirosaki 036-8561

[2]Research and Development Division, Nippon Chemical Industrial Co., Ltd., Koto-ku, Tokyo 136-8515

[3]JEOL Ltd., Akishima, Tokyo 195-8558

Received August 6, 2009; E-mail: hideosaw@cc.hirosaki-u.ac.jp

Novel cross-linked fluoroalkyl end-capped trimethoxyvinylsilane oligomeric nanoparticles [R_F–(VM-SiO_2)$_n$–R_F]-encapsulated 1,1′-bi(2-naphthol) (BINOL) were prepared by the hydrolysis of fluoroalkyl end-capped trimethoxyvinylsilane oligomer in the presence of BINOL under alkaline conditions. R_F–(VM-SiO_2)$_n$–R_F-encapsulated BINOL nanocomposite thus obtained afforded no weight loss corresponding to the presence of BINOL in the composite at 800 °C. Interestingly, R_F–(VM-SiO_2)$_n$–R_F/BINOL nanocomposite did not show absorption peaks before calcination however this nanocomposite was found to exhibit similar absorption and fluorescence peaks to those of the parent BINOL after calcination at 800 °C. More interestingly, R_F–(VM-SiO_2)$_n$–R_F/BINOL nanocomposite after calcination exhibited a releasing characteristic into methanol although before calcination this nanocomposite showed no such characteristic at all. In particular, FT-IR spectra of the released molecules showed typical bands related to both the parent BINOL and silica gel, indicating that the released guest molecules should be thermally stable even at 800 °C through the architecture of rigid BINOL-containing silica gel matrices.

Fluorinated polymers such as poly(tetrafluoroethylene) and poly(vinylidene fluoride) can afford extraordinary thermal and oxidative stability due to the bond-strengthening effect of fluorine for C–C and C–F bonds in highly fluorinated compounds, compared to that of the corresponding nonfluorinated materials.[1–7] Therefore, from the developmental viewpoints of additional high-performance thermally resistant materials, hybridizations of the fluorinated polymers with metal alkoxides are of particular interest. Some studies of the hybridization of fluorinated polymers with alkoxysilanes have been reported however the thermal stability of these hybrids is in general inferior to that of the original silica gels.[8–11] In a variety of fluorinated polymers, we have hitherto reported that fluoroalkyl end-capped oligomers are attractive functional materials, because they exhibit various unique properties such as high solubility, surface active properties, biological activities, and nanometer size-controlled self-assembled molecular aggregates which cannot be achieved by the corresponding non-fluorinated and randomly fluoroalkylated polymers.[6,7] In these fluoroalkyl end-capped oligomers, fluoroalkyl end-capped trimethoxyvinylsilane oligomers are of particular interest due to exhibiting higher surface active characteristics compared to the traditional fluoroalkylated silane coupling agents [R_F–$CH_2CH_2Si(OR)_3$; R_F = fluoroalkyl groups].[12] In view of the development of new fluorinated polymer hybrid materials, it is of particular interest to explore new fluoroalkyl end-capped trimethoxyvinylsilane oligomeric nanocomposites which could exhibit improved properties compared to those of the parent fluorinated oligomers. In fact, we have very recently found that the hydrolysis of fluoroalkyl end-capped trimethoxyvinylsilane oligomer under alkaline conditions can afford the corresponding nanometer size-controlled fluorinated trimethoxyvinylsilane oligomer/silica composites.[13] We have also found that a modified glass surface treated with these fluorinated nanocomposites can exhibit complete super-hydrophobicity (water contact angle: 180°).[13] During our comprehensive studies of the preparation and properties of fluoroalkyl end-capped trimethoxyvinylsilane oligomer/silica nanocomposites, fluoroalkyl end-capped trimethoxyvinylsilane oligomer/1,1′-bi(2-naphthol) (BINOL)/silica nanocomposite [R_F–(VM-SiO_2)$_n$–R_F/BINOL] have been prepraed by the hydrolysis of the corresponding oligomer in the presence of BINOL under alkaline conditions. R_F–(VM-SiO_2)$_n$–R_F/BINOL nanocomposite thus obtained was found to afford a clear weight loss at 800 °C, which corresponds to the content of fluorinated oligomer in the composite. However, unexpectedly, we have discovered that R_F–(VM-SiO_2)$_n$–R_F/BINOL nanocomposite exhibits no weight loss corresponding to the presence of BINOL in the composite at 800 °C under atmospheric conditions. These findings will be described herein.

Results and Discussion

Fluoroalkyl end-capped trimethoxyvinylsilane oligomer suffered hydrolysis under alkaline conditions in the presence of

Published on the web December 23, 2009; doi:10.1246/bcsj.20090204

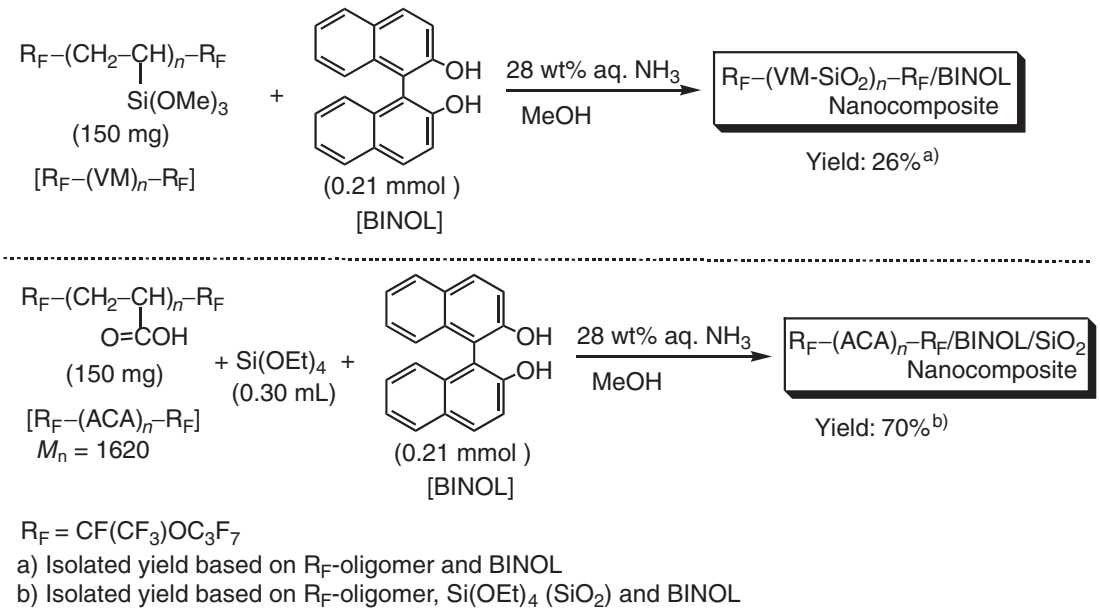

Scheme 1. Preparation of fluorinated oligomers/BINOL nanocomposites.

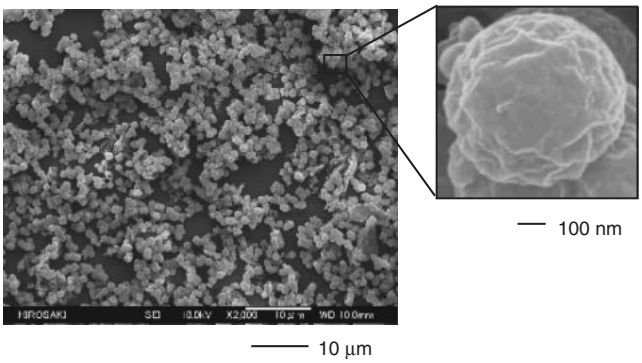

Figure 1. FE-SEM images of methanol solution of R_F–$(VM\text{-}SiO_2)_n$–R_F/BINOL nanocomposite before calcination.

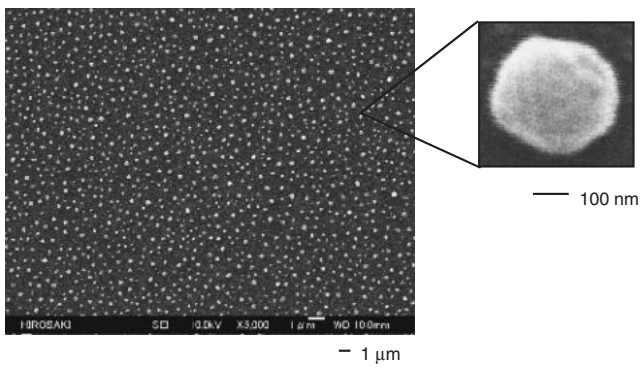

Figure 2. FE-SEM images of methanol solution of R_F–$(ACA)_n$–R_F/BINOL/SiO_2 nanocomposite before calcination.

1,1′-bi(2-naphthol) (BINOL) to afford R_F–$(VM\text{-}SiO_2)_n$–R_F/BINOL nanocomposite in 26% isolated yield. Similarly, we have prepared fluoroalkyl end-capped acrylic acid oligomer [R_F–$(ACA)_n$–R_F]/BINOL/SiO_2 nanocomposite under similar conditions, for comparison. These results are shown in Scheme 1.

The obtained R_F–$(VM\text{-}SiO_2)_n$–R_F/BINOL nanocomposite has good dispersibility in traditional organic solvents such as methanol, ethanol, *i*-propyl alcohol (*i*-PrOH), chloroform, tetrahydrofuran (THF), 1,2-dichloroethane (DE), hexane, dimethyl sulfoxide (DMSO), *N,N*-dimethylformamide (DMF), and fluorinated aliphatic solvents (AK-225: 1:1 mixed solvents of 1,1-dichloro-2,2,3,3,3-pentafluoropropane and 1,3-dichloro-1,2,2,3,3-pentafluoropropane) except for water. On the other hand, R_F–$(ACA)_n$–R_F/BINOL/SiO_2 nanocomposite was found to exhibit higher dispersibility not only in water but also in these organic solvents. Dynamic light-scattering (DLS) measurements at 25 °C show that the size of R_F–$(VM\text{-}SiO_2)_n$–R_F/BINOL nanocomposite and R_F–$(ACA)_n$–R_F/BINOL/SiO_2 nanocomposite in methanol were 840 ± 210 and 188 ± 45.0 nm, respectively. We have measured the field emission scanning electron micrograph (FE-SEM) of methanol solutions of R_F–$(VM\text{-}SiO_2)_n$–R_F/BINOL nanocomposite and R_F–$(ACA)_n$–R_F/BINOL/SiO_2 nanocomposite, and the results were shown in Figures 1 and 2. Electron micrographs also showed the formation of fluorinated composite nanoparticles with a mean diameter of 925 and 188 nm, respectively, and similar values were obtained in DLS and FE-SEM measurements.

Thermal stability of fluorinated nanocomposites in Scheme 1 was studied by thermogravimetric analyses (TGA), in which the weight loss of these nanocomposites was measured by raising the temperature around 800 °C (the heating rate: 10 °C min^{-1}) in air atmosphere, and the results are shown in Figures 3 and 4.

The parent BINOL decomposed completely around 300 °C (Figure 3A-c), and the weight of parent R_F–$(ACA)_n$–R_F oligomer markedly dropped around 250 °C and decomposed gradually, reaching 0% around 540 °C (data not shown). A similar tendency was observed in R_F–$(ACA)_n$–R_F/SiO_2 nanocomposite, and a constant value for weight loss was

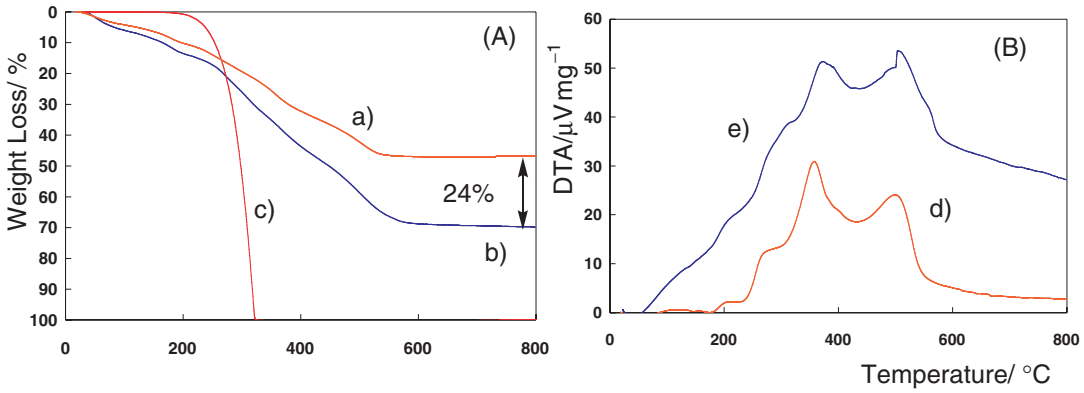

Figure 3. Thermogravimetric analyses [TGA (A)] and differential thermal analyses [DTA (B)] of R_F–$(ACA)_n$–R_F/BINOL/SiO_2 nanocomposite, R_F–$(ACA)_n$–R_F/SiO_2 nanocomposite, and BINOL. a), d) R_F–$(ACA)_n$–R_F/SiO_2 nanocomposites; b), e) R_F–$(ACA)_n$–R_F/BINOL/SiO_2 nanocomposites; and c) parent BINOL.

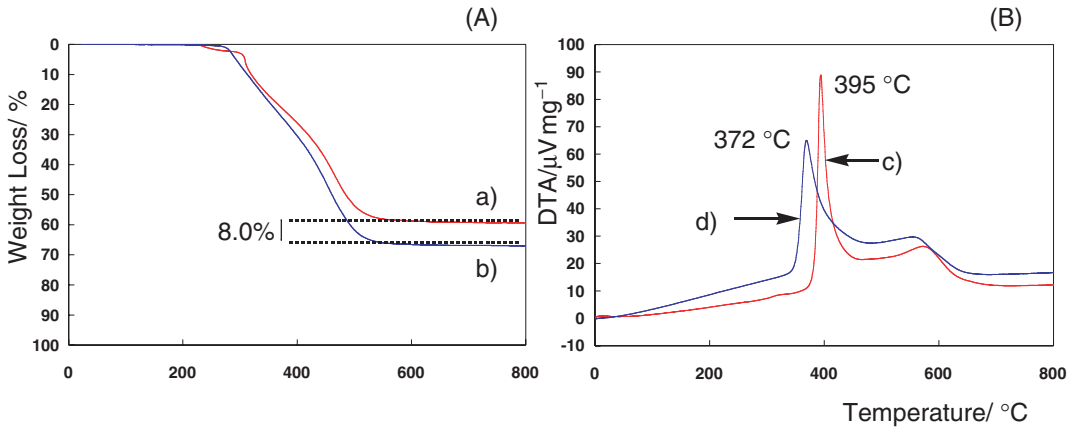

Figure 4. TGA (A) and DTA (B) of R_F–$(VM\text{-}SiO_2)_n$–R_F/BINOL nanocomposite and R_F–$(VM\text{-}SiO_2)_n$–R_F nanocomposite. a), c) R_F–$(VM\text{-}SiO_2)_n$–R_F/BINOL nanocomposites and b), d) R_F–$(VM\text{-}SiO_2)_n$–R_F nanocomposites.

observed above 540 °C, indicating that this nanocomposite could possess silica gel nanoparticles (Figure 3A-a). R_F–$(ACA)_n$–R_F/BINOL/SiO_2 nanocomposite (Figure 3A-b) decomposed effectively at 800 °C to exhibit higher weight loss compared to R_F–$(ACA)_n$–R_F/SiO_2 nanocomposite, indicating that the content of BINOL in this composite is 24%.

On the other hand, unexpectedly, we did not observe effective weight loss of R_F–$(VM\text{-}SiO_2)_n$–R_F/BINOL nanocomposite corresponding to the presence of BINOL at all from room temperature to 800 °C (Figure 3A-a), compared to the corresponding R_F–$(VM\text{-}SiO_2)_n$–R_F nanocomposite (Figure 3A-b), although the R_F–$(VM\text{-}SiO_2)_n$–R_F/BINOL nanocomposite contains BINOL which decomposes completely around 300 °C. Thus, the content of BINOL in the composite was estimated to be 8.0% by TGA measurements.

DTA (differential thermal analyses) for R_F–$(ACA)_n$–R_F/BINOL/SiO_2 nanocomposite in air (heating rate: 10 °C min^{-1}) showed that as the temperature reached around 300 °C, exothermic phenomenon occurred, and exothermic peaks appeared around 380 and 500 °C, respectively, which may be caused by the decomposition of R_F–$(ACA)_n$–R_F oligomer in the composite (Figure 3B-e). A similar result was obtained in the case of the R_F–$(ACA)_n$–R_F/SiO_2 nanocomposite (Figure 3B-d), indicating that the usual composite reaction of R_F–$(ACA)_n$–R_F oligomer with silica gel (tetraethoxysilane) in the presence of BINOL should proceed smoothly under alkaline conditions.

On the other hand, DTA for R_F–$(VM\text{-}SiO_2)_n$–R_F/BINOL nanocomposite showed a clear exothermic peak at 395 °C (Figure 4B-c). This exothermic temperature is much higher than that (372 °C) of R_F–$(VM\text{-}SiO_2)_n$–R_F nanocomposite (Figure 4B-d), indicating that BINOL should be encapsulated quite effectively as a guest molecule into the nanometer size-controlled R_F–$(VM\text{-}SiO_2)_n$–R_F nanocomposite matrices through the molecular-level combination, which is due to the intermolecular hydrogen-bonding interaction between the hydroxy groups in BINOL and residual silanol groups in the composite matrices.

Interestingly, the average particle size [457 ± 109 nm (determined by DLS) of R_F–$(VM\text{-}SiO_2)_n$–R_F/BINOL nanocomposite after calcination was almost the same as that (840 ± 210 nm) before calcination, and exhibited good dispersibility and stability in a variety of organic solvents.

FE-SEM of R_F–$(VM\text{-}SiO_2)_n$–R_F/BINOL nanocomposite after calcination also showed the formation of fine particles with a mean diameter of 777 nm (Figure 5), as well as that before calcination (Figure 1). Interestingly, we observed a relatively smooth particle surface after calcinations (Figure 5).

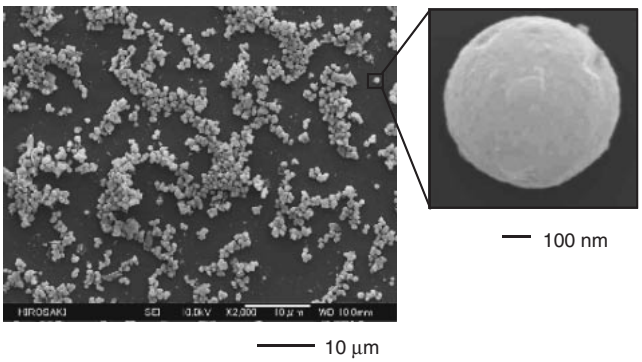

Figure 5. FE-SEM images of methanol solution of R_F–$(VM\text{-}SiO_2)_n$–R_F/BINOL nanocomposites after calcination.

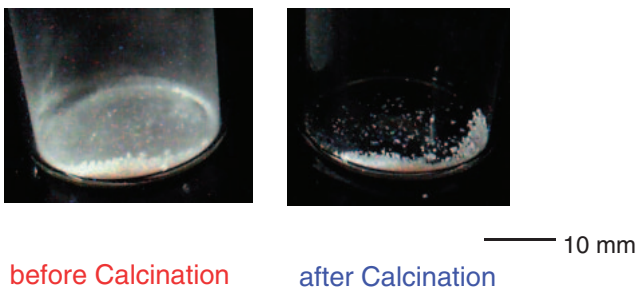

Figure 6. Photographs of R_F–$(VM\text{-}SiO_2)_n$–R_F/BINOL nanocomposite powders before and after calcination.

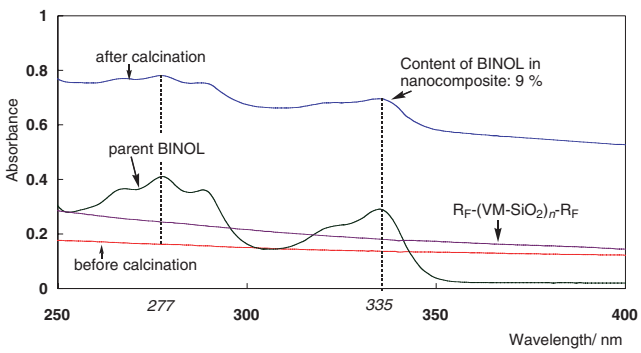

Figure 7. UV–vis spectra of 0.2 g dm^{-3} R_F–$(VM\text{-}SiO_2)_n$–R_F/BINOL nanocomposites before and after calcination in methanol, 0.2 g dm^{-3} R_F–$(VM\text{-}SiO_2)_n$–R_F nanocomposite in methanol, and parent BINOL (10 mg dm^{-3}) in methanol.

In addition, it was demonstrated that the appearance of white nanocomposite powders did not change at all before and after calcination at 800 °C as shown in Figure 6.

In order to clarify the presence of BINOL in the R_F–$(VM\text{-}SiO_2)_n$–R_F/BINOL nanocomposite, we have studied the UV–vis spectra of well dispersed methanol solutions of R_F–$(VM\text{-}SiO_2)_n$–R_F/BINOL nanocomposite, and the results are shown in Figure 7.

As shown in Figure 7, we were unable to observe absorption peaks related to BINOL in the nanocomposite before calcination, as well as the parent R_F–$(VM\text{-}SiO_2)_n$–R_F nanocomposite however unexpectedly, this nanocomposite after calcination at 800 °C was displayed absorption peaks which are quite similar to those of parent BINOL. Furthermore, the content of BINOL in the nanocomposite after calcination was estimated to be 9%

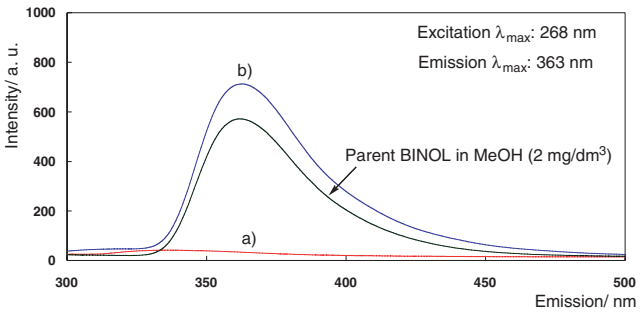

Figure 8. Relative fluorescent intensity of 0.20 g dm^{-3} R_F–$(VM\text{-}SiO_2)_n$–R_F/BINOL/nanocomposites before (a) and after (b) calcination in methanol.

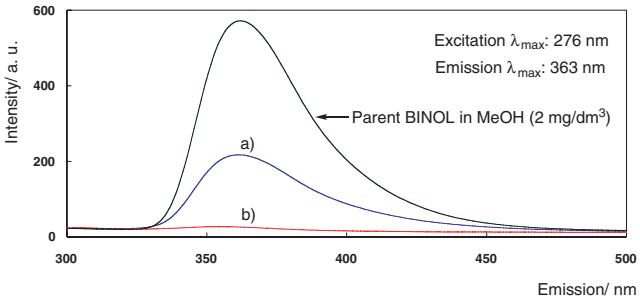

Figure 9. Relative fluorescent intensity of 0.20 g dm^{-3} R_F–$(ACA)_n$–R_F/BINOL/SiO_2 nanocomposites before (a) and after (b) calcination in methanol.

by the use of the absorbance at 335 nm of the parent BINOL. This value is almost the same as that of TGA measurements as in Figure 4.

In this way, we have succeeded in observing the clear absorption spectra of R_F–$(VM\text{-}SiO_2)_n$–R_F/BINOL nanocomposite after calcination. Thus, we tried to study the fluorescence spectra of this nanocomposite, and the results are shown in Figure 8.

Fluorescence spectra was not observed at all in the nanocomposite before calcination (Figure 8a) as well as the absorption spectra as in Figure 7 however R_F–$(VM\text{-}SiO_2)_n$–R_F/BINOL nanocomposite after calcination (Figure 8b) are excited ($\lambda = 268$ nm) into the BINOL intense absorption bands in the UV–vis region, it emits fluorescence with a peak maximum around 363 nm in methanol solution. A similar result was obtained in the parent BINOL (Figure 8).

On the other hand, R_F–$(ACA)_n$–R_F/BINOL/SiO_2 nanocomposite, which exhibits a clear weight loss at 800 °C corresponding to the presence of BINOL in the composite, was found to afford a fluorescence peak around 363 nm before calcination (Figure 9a), however this fluorescence peak completely disappeared after calcination at 800 °C (Figure 9b).

Relative fluorescence intensity of BINOL [content of BINOL in the composite: 8% (determined by TGA measurements)] in the R_F–$(VM\text{-}SiO_2)_n$–R_F/BINOL nanocomposite (0.2 g dm^{-3}) after calcination based on the parent BINOL (2 mg dm^{-3}) is 89/512 (0.174). In contrast, relative fluorescence intensity of BINOL [content of BINOL in the composite: 24% (determined by TGA measurements)] in the R_F–$(ACA)_n$–R_F/BINOL/SiO_2 nanocomposite (0.2 g dm^{-3}) before calci-

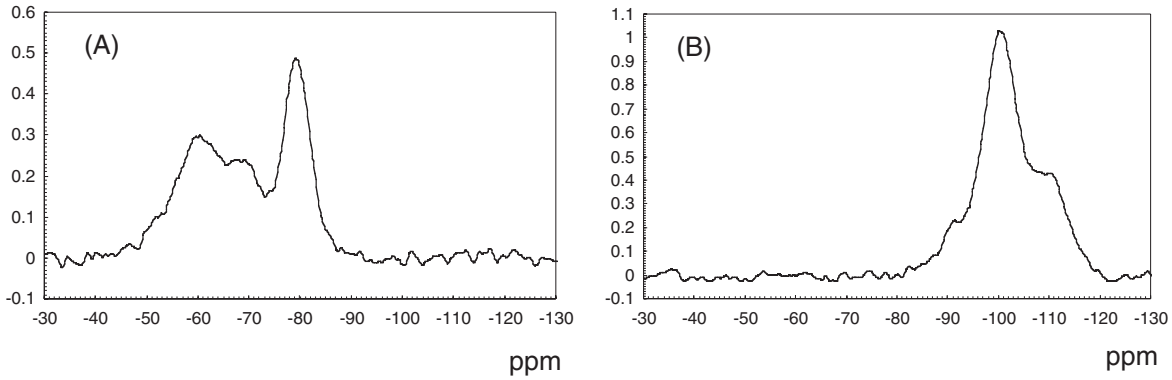

Figure 10. ^{29}Si CP/MAS NMR spectra of R_F–(VM-SiO_2)$_n$–R_F/BINOL nanocomposites before (A) and after (B) calcination determined by JNM-ECA500 with 4.0 mm CP/MAS probe.

nation based on the parent BINOL (2 mg dm^{-3}) is 9/571 (0.016). Thus, we obtained a higher relative fluorescent intensity of BINOL in the R_F–(VM-SiO_2)$_n$–R_F/BINOL nanocomposite after calcinations about 10-fold relative to that of R_F–(ACA)$_n$–R_F/BINOL/SiO_2 nanocomposite before calcination. This finding suggests that the inside of R_F–(VM-SiO_2)$_n$–R_F/BINOL nanocomposite cores consist of a solvophobic environment, and under such specific conditions, BINOL could interact strongly as a guest molecule with the nanocomposite cores through the intermolecular hydrogen-bonding interaction between hydroxy groups in BINOL and the residual silanol groups in the composites. The molecular motions of BINOL in the nanocomposites would be remarkably restricted in the nanocomposite cores to exhibit no light absorption before calcination, compared to that of R_F–(ACA)$_n$–R_F/BINOL/SiO_2 nanocomposite. Hence, such effectively restricted BINOL guest molecule could afford a clear fluorescence spectra related to BINOL in the composite only after calcination at 800 °C. In fact, we have very recently found that cross-linked fluoroalkyl end-capped oligomeric nanocomposites possessing aromatic siloxane segments, which were prepared by the hydrolysis of alkoxysilanes containing aromatic groups in the presence of the corresponding oligomers under alkaline conditions, can exhibit much higher fluorescence than the parent alkoxysilanes containing aromatic groups due to the effective restriction of aromatic segments in the cross-linked fluorinated oligomeric nanocomposite cores.[14] Similarly, it is well-known that silicon-bridged biaryls, of which both the silicon atoms and benzene rings are significantly deformed from the normal tetrahedral and hexagon shapes, respectively, can emit extraordinarily higher fluorescence due to the perfect planarity of the molecular framework.[15–17] Inagaki et al. have also reported that naphthylene-bridged mesoporus organosilicas can emit a higher fluorescence due to the effective restriction of the rotational motion of the naphthalene ring around the Si–C bond axis in the mesoporus silica network.[18,19]

^{29}Si magic-angle spinning (MAS) NMR spectra of R_F–(VM-SiO_2)$_n$–R_F/BINOL nanocomposite before and after calcination at 800 °C have been measured in order to clarify this interesting thermostability in R_F–(VM-SiO_2)$_n$–R_F/BINOL nanocomposite, and the results are shown in Figure 10.

In the R_F–(VM-SiO_2)$_n$–R_F/BINOL nanocomposite before calcination, the chemical shifts observed around −60, −67 and −80 ppm were assigned to Q^4, Q^3, and Q^2 species (Figure 10a). In contrast, these signals have completely disappeared after calcination of this nanocomposite, and a relatively sharp peak around −100 ppm (Q^1) was observed with a shoulder peak (ca. −110 ppm (Q^0)) (Figure 10b). In the nomenclature used for ^{29}Si NMR spectroscopy for the classification of the peaks by the degree of condensation, the noncondensation is indicated by the annotation Q^0, and a silicon bridged to only one other silicon atom is indicated by the annotation Q^1. The annotation of Q^2, Q^3, and Q^4 are used for silicon directly attached to two, three, and four silicon–oxygen bonds, respectively.[20] These findings suggest that the encapsulated BINOL molecules in the R_F–(VM-SiO_2)$_n$–R_F/BINOL nanocomposite cores can be tightly attached to one silicon–oxygen bond even after caclination at 800 °C.

We have tested our present R_F–(VM-SiO_2)$_n$–R_F/BINOL nanocomposite after calcination at 800 °C for the release of BINOL from the nanocomposite into methanol. We have succeeded in isolating the released guest molecules in methanol after stirring the methanol solution containing this composite at room temperature for 1 day, although such releasing of the nanocomposite before calcination at 800 °C into methanol was not observed at all under similar conditions. FT-IR spectra of R_F–(VM-SiO_2)$_n$–R_F/BINOL nanocomposite before calcination at 800 °C exhibited the typical bands of both fluoroalkyl end-capped trimethoxyvinylsilane oligomer and silica gel around 1334 (CF_3), 1238 (CF_2), and 1203–1065 cm^{-1} (SiO_2) (Figure 11a). After calcination, the bands related to the fluorinated oligomer completely disappeared to exhibit bands related to only the parent silica gel (Figure 11b). On the other hand, after centrifugal separation (2000 rpm/30 min) of the calcinated R_F–(VM-SiO_2)$_n$–R_F/BINOL nanocomposite methanol solutions, we have easily isolated the white powders, whose FT-IR spectra were characterized by the parent silica gel (Figure 11d). However interestingly, the released guest molecules, which were isolated from this supernatant solution, showed typical bands related to not only 1604, 1412, 1134, and 775 cm^{-1} corresponding to BINOL (Figure 11e) but also silica gel (1049 cm^{-1}) (Figure 11c), indicating that the released BINOL guest molecule would be nonflammable even at 800 °C through the architecture of rigid BINOL-containing silica gel matrices during the nanocomposite process of R_F–(VM)$_n$–R_F oligomer in the presence of BINOL under alkaline conditions.

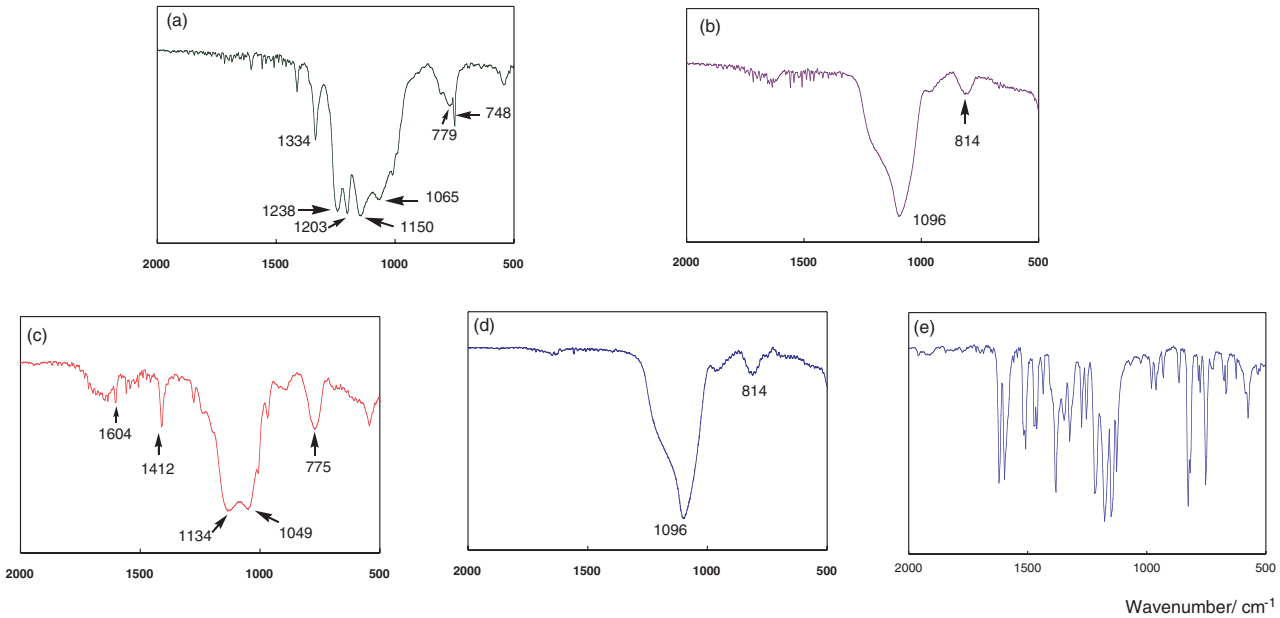

Figure 11. FT-IR spectra of R_F–(VM-SiO_2)$_n$–R_F/BINOL nanocomposite before (a) and after (b) calcination, released guest molecule (c), precipitated powders after centrifugal separtion (d), and parent BINOL (e).

Conclusion

We have succeeded in preparing R_F–(VM-SiO_2)$_n$–R_F/BINOL nanocomposite by the hydrolysis of fluoroalkyl end-capped trimethoxyvinylsilane oligomer in the presence of BINOL under alkaline conditions. R_F–(ACA)$_n$–R_F/BINOL/SiO_2 nanocomposite was also prepared under similar conditions, for comparison. R_F–(ACA)$_n$–R_F/BINOL/SiO_2 nanocomposite exhibited a clear weight loss corresponding to the presence of BINOL in the nanocomposite at 800 °C however unexpectedly, R_F–(VM-SiO_2)$_n$–R_F/BINOL nanocomposite showed no weight loss corresponding to the presence of BINOL in the composite after calcination at 800 °C. Interestingly, R_F–(VM-SiO_2)$_n$–R_F/BINOL nanocomposite did not exhibit the absorption peaks before calcination however this nanocomposite exhibited similar absorption and fluorescence peaks to those of the parent BINOL after calcination. More interestingly, R_F–(VM-SiO_2)$_n$–R_F/BINOL nanocomposite after calcination at 800 °C showed release into methanol, and FT-IR spectra of the released molecules showed the typical bands related to both the parent BINOL and silica gel, indicating that the released guest molecule should be nonflammable even at 800 °C through the architecture of rigid BINOL-containing silica gel matrices.

Experimental

Ultraviolet–visible (UV–vis) spectra were measured with a Shimadzu UV-1600 UV–vis spectrophotometer (Kyoto, Japan). Dynamic light-scattering (DLS) were measured by using an Otsuka Electronics DLS-7000 HL (Tokyo, Japan). Fluorescence spectra were measured by using a JASCO FP-6300 (Tokyo, Japan). Fourier-transform infrared (FTIR) spectra were measured using Shimadzu FTIR-8400 FT-IR spectrophotometer (Kyoto, Japan). Field-emission scanning electron microscopy (FE-SEM) images were measured by using a JEOL JSM-5300 (Tokyo, Japan). Thermal analyses were recorded on a Bruker axs TG-DTA2000SA differential thermobalance (Kanagawa, Japan). ^{29}Si magic-angle spinning (MAS) NMR spectra were measured at room temperature using a JEOL JNM-ECA500 with a 4.0 mm CP/MAS probe. Fluoroalkyl end-capped trimethoxyvinylsilane oligomer and acrylic acid oligomer were prepared by reaction of fluoroalkanoyl peroxide with the corresponding monomers according to our previously reported methods.[12,21]

Preparation of R_F–(VM-SiO_2)$_n$–R_F/BINOL Nanocomposite. A typical procedure for the preparation of R_F–(VM-SiO_2)$_n$–R_F/BINOL nanocomposite is as follows: To methanol solution (12.5 mL) containing fluoroalkyl end-capped trimethoxyvinylsilane oligomer [150 mg; R_F–[CH_2CHSi(OMe)$_3$]$_n$–R_F: R_F–(VM)$_n$–R_F; R_F = CF(CF_3)OC_3F_7; n = 2 and 3] and BINOL (0.21 mmol), was added 28% aqueous ammonia solution (2.4 mL). The mixture was stirred with a magnetic stirring bar at room temperature for 1 day. After centrifugal separation of this solution, the obtained products were washed well with methanol several times, and dried in vacuo to afford the expected white powdery product (78 mg). Fluoroalkyl end-capped acrylic acid oligomer [R_F–(CH_2CHCOOH)$_n$–R_F; R_F = CF(CF_3)OC_3F_7; M_n = 1620]/BINOL/silica nanocomposite was prepared under similar conditions (Scheme 1).

References

1 W. R. Dolbier, Jr., *J. Fluorine Chem.* **2005**, *126*, 157.
2 *Modern Fluoropolymers*, ed. by J. Scheirs, Wiley, Chichester, **1997**.
3 B. Ameduri, B. Boutevin, *Well-Architectured Fluoropolymers, Synthesis, Properties and Applications*, Elsevier, Amsterdam, **2004**.
4 H. Sawada, *Chem. Rev.* **1996**, *96*, 1779.
5 H. Sawada, *J. Fluorine Chem.* **2000**, *105*, 219.
6 H. Sawada, *Prog. Polym. Sci.* **2007**, *32*, 509.
7 H. Sawada, *Polym. J.* **2007**, *39*, 637.
8 M. A. Harmer, W. E. Farneth, Q. Sun, *J. Am. Chem. Soc.*

1996, *118*, 7708.
9 J. W. Cho, K. I. Sul, *Fibers Polym.* **2001**, *2*, 135.
10 S. Yano, N. Okubo, K. Takahashi, *Macromol. Symp.* **1996**, *108*, 270.
11 P. Fabbri, M. Messori, M. Montecchi, S. Nannarone, L. Pasquali, F. Pilati, C. Tonelli, M. Toselli, *Polymer* **2006**, *47*, 1055.
12 H. Sawada, M. Nakayama, *J. Chem. Soc., Chem. Commun.* **1991**, 677.
13 H. Sawada, T. Suzuki, H. Takashima, K. Takishita, *Colloid Polym. Sci.* **2008**, *286*, 1569.
14 Y. Goto, H. Sawada, *Colloid Polym. Sci.* **2009**, *287*, 1317.
15 M. Shimizu, H. Tatsumi, K. Mochida, K. Oda, T. Hiyama, *Chem. Asian J.* **2008**, *3*, 1238.
16 J. Chen, Y. Cao, *Macromol. Rapid Commun.* **2007**, *28*, 1714.
17 M. Shimizu, K. Mochida, T. Hiyama, *Angew. Chem.* **2008**, *120*, 9906.
18 N. Mizoshita, Y. Goto, T. Tani, S. Inagaki, *Adv. Funct. Mater.* **2008**, *18*, 3699.
19 N. Mizoshita, Y. Goto, M. P. Kapoor, T. Shimada, T. Tani, S. Inagaki, *Chem.—Eur. J.* **2008**, *15*, 219.
20 Y.-C. Chen, C.-C. Tsai, Y.-D. Lee, *J. Polym. Sci., Part A: Polym. Chem.* **2004**, *42*, 1789.
21 H. Sawada, Y.-F. Gong, Y. Minoshima, T. Matsumoto, M. Nakayama, M. Kosugi, T. Migita, *J. Chem. Soc., Chem. Commun.* **1992**, 537.